Research article

Atrazine degradation through a heterogeneous dual-effect process using Fe–TiO$_2$-allophane catalysts under sunlight

Jorge Castro-Rojas [a,b,i], Pablo Jofré-Dupre [c], Néstor Escalona [d,e], Elodie Blanco [d,e,f], María Soledad Ureta-Zañartu [g], Maria Luz Mora [h,i,*], Elizabeth Garrido-Ramírez [c,j,**]

[a] Programa de Doctorado en Ciencias de Recursos Naturales, Universidad de La Frontera, Avenida Francisco Salazar 01145, PO Box 54-D, Temuco, Chile

[b] Department of Agricultural Sciences, University of Naples Federico II, Via Università 100, Portici, 80055, Italy

[c] Escuela de Ciencias Ambientales y Sustentabilidad, Universidad Andres Bello, República 440, Santiago, 83270255, Chile

[d] Department of Chemical Engineering and Bioprocesses, Pontificia Universidad Católica de Chile, Vicuña Mackenna 4860, Macul, Santiago, 8320000, Chile

[e] Millennium Nucleus in Catalytic Processes towards Sustainable Chemistry (CSC), ANID Millennium Science Initiative Program, Santiago, 8320000, Chile

[f] Department of Construction Engineering and Management, Pontificia Universidad Católica de Chile, Vicuña Mackenna 4860, Macul, Santiago, 8320000, Chile

[g] Departamento de Ciencias del Ambiente, Facultad de Química y Biología, Universidad de Santiago de Chile, Av. Libertador Bernardo O'Higgins 3363, casilla 40, correo 33, Santiago, Chile

[h] Center of Plant Soil Interaction and Natural Resources Biotechnology, Scientific and Technological Bioresource Nucleus (BIOREN-UFRO), Universidad de La Frontera, Avenida Francisco Salazar 01145, 4780000, Temuco, Chile

[i] Departamento de Ciencias Químicas y Recursos Naturales, Facultad de Ingeniería y Ciencias, Universidad de La Frontera, Avenida Francisco Salazar 01145, PO Box 54-D, Temuco, Chile

[j] Centro de Investigación para la Sustentabilidad (CIS), Facultad de Ciencias de La Vida, Universidad Andres Bello, Republica 440, Santiago, 8327055, Chile

ARTICLE INFO

ABSTRACT

This study investigated the novel application of Fe–TiO$_2$-allophane catalysts with 6.0 % w/w of iron oxide and two TiO$_2$ proportions (10 % and 30 % w/w) for degrading atrazine (ATZ) using the heterogeneous dual-effect (HDE) process under sunlight. Comparative analyses with Fe-allophane and TiO$_2$-allophane catalysts were conducted in both photocatalysis (PC) and HDE processes. FTIR spectra reveal the unique hydrous feldspathoids structure of allophane, showing evidence of new bond formation between Si–O groups of allophane clays and iron hydroxyl species, as well as Si–O–Ti bonds that intensified with higher TiO$_2$ content. The catalysts exhibited an anatase structure. In Fe–TiO$_2$-allophane catalysts, iron oxide was incorporated through the substitution of Ti^{4+} by Fe^{3+} in the anatase crystal lattice and precipitation on the surface of allophane clays, forming small iron oxide particles. Allophane clays reduced the agglomeration and particle size of TiO$_2$, resulting in an enhanced specific surface area and pore volume for all catalysts. Iron oxide incorporation decreased the band gap, broadening the photoresponse to visible light. In the PC process, TiO$_2$-allophane achieves 90 % ATZ degradation, attributed to radical species from the UV component of sunlight. In the HDE process, Fe–TiO$_2$-allophane catalysts exhibit synergistic effects, particularly with 30 % w/w TiO$_2$, achieving 100 % ATZ degradation and 85 % COD

* Corresponding author.
** Corresponding author.
E-mail addresses: mariluz.mora@ufrontera.cl (M.L. Mora), elizabeth.garrido@unab.cl (E. Garrido-Ramírez).

removal, with shorter reaction time as TiO$_2$ percentage increased. The HDE process was performed under less acidic conditions, achieving complete ATZ degradation after 6 h without iron leaching. Consequently, Fe–TiO$_2$-allophane catalysts are proposed as a promising alternative for degrading emerging pollutants under environmentally friendly conditions.

1. Introduction

Agricultural practices, industrial discharges, and human activities play an essential role in the release of a wide variety of emerging pollutants into watercourses. These pollutants include pharmaceuticals, hormones, steroids, disinfection by-products, personal care products, household products, and pesticides, among others [1]. Consequently, several authors have reviewed the scientific literature regarding the occurrence of emerging pollutants in aquatic ecosystems, providing evidence that the number of studies reporting the presence of emerging pollutants has increased in recent years [1–4]. The main problem with these kinds of pollutants is the lack of knowledge of their effects on human health and the environment, mainly in the medium or long term [5,6]. One example is atrazine (ATZ), which has been widely reported as an emergent pollutant in different source waters [4,7–9]. For instance, Peña Guzman et al. [4], reported ATZ concentrations ranging from 8 to 55 ng L^{-1} in surface water and from 1.1 to 74 ng L^{-1} in drinking water treatment plants, both in Latin America. On the other hand, Triassi et al. [7], detected ATZ concentrations ranging from 18.1 to 105.5 ng L^{-1} in a river estuary of Southern Italy, while Climent et al. [8], reported ATZ concentrations ranging from 55 to 149 ng L^{-1} in a river in the South of Chile. ATZ is a selective herbicide widely used in Chile for controlling broadleaf and grassy weeds in corn and forestry plantations. ATZ is an endocrine disruptor [10], and due to its physicochemical properties, it remains in the environment for a long time. ATZ is a recalcitrant organic pollutant, which implies that its degradation using conventional wastewater treatments is difficult [11,12]. Therefore, it is necessary to develop new wastewater treatments able to remove emerging pollutants from aquatic systems in an environmentally friendly way. In this sense, advanced oxidation processes (AOPs) appear to be a promising alternative. AOPs are based on the generation of radical species to oxidize organic matter. For that purpose, different strategies have been used, such as the use of ozone, Fenton-based processes, photocatalysis, and electrochemical processes, among others [5,13–16].

The Bansal research group [17–19] first proposed the AOP process called the "dual-effect," which combines the advantages of the photo Fenton and photocatalysis processes. In this process, a synergetic effect has been reported by enhancing the degradation efficiency and reducing the time of photocatalytic reactions compared with both processes separately [19–21]. To perform a heterogeneous dual-effect process, it is necessary to use a solid catalyst with an active metal for the Fenton reaction (for example, Fe(II)/Fe(III) species) able to react with H$_2$O$_2$ to generate the hydroxyl radical through a Fenton-like reaction [13]. Additional hydroxyl radicals can be generated using UV or sunlight due to the photolysis of Fe(OH)$^{2+}$ and regeneration of Fe(II) in a photo Fenton process [22,23]. Simultaneously, it is necessary to incorporate a semiconductor able to be excited by photons with an energy greater than its bandgap to generate electron-hole pair reactions [24,25]. For that purpose, the most widely used photocatalyst is TiO$_2$ due to its photostability, high photocatalytic activity, reusability, low cost, and nontoxicity [16,26]. However, its application in wastewater treatment is limited because its photoresponse is only in the ultraviolet region of the electromagnetic spectrum [27–29]. Meanwhile, the solar spectrum typically contains about 4 % UV light; therefore, the sunlight cannot be efficiently used in the photocatalytic process [30]. To overcome this drawback, studies have shown that the doping of TiO$_2$ with other narrow bandgap materials, such as iron oxide, could reduce its bandgap and minimize e$^-$/h$^+$ recombination rate [16,21,31,32]. In this way, it is possible to degrade emerging pollutants using photocatalysts containing both iron oxide and TiO$_2$ through a heterogeneous dual-effect process under sunlight. In addition, the use of clay minerals as support for both iron oxide and TiO$_2$ could reduce the agglomeration of TiO$_2$ and enhance organic pollutant degradation by photocatalysis [29]. Clays exhibit a high surface area, large pore volume, chemical stability, and good mechanical properties that improve the interaction between the active sites of photocatalysts and organic pollutants [33].

Therefore, this work aims to use Fe–TiO$_2$-allophane nanocomposites as photocatalysts to degrade ATZ by a heterogeneous dual-effect process under natural sunlight. Allophane is a clay mineral of widespread occurrence in volcanic ash soils (mostly Andisols). Their unitary structure consists of hollow spherules that are highly porous with a diameter in the nanoscale range (3–5 nm) [34–36]. These clays occur in association with poorly crystalline iron oxides, mainly ferrihydrite, which is often found as coatings of allophane particles [37]. Due to allophane properties, such as a large specific BET surface area, unique structure, and high porosity, synthetic copper and iron oxide-supported allophane with a similar structure to hydrous feldspathoid were reported as active catalysts for the oxidation of phenol and atrazine by the heterogeneous Fenton reaction [38] and heterogeneous electro-Fenton process [39,40]. Nishikiori et al. [41], proposed for the first time the combination of allophane clays with TiO$_2$ to study the degradation of trichloroethylene under UV irradiation. However, to the best of our knowledge, the simultaneous incorporation of iron oxide and titanium dioxide on allophane clay and their ability to remove emerging pollutants by the heterogeneous dual-effect process under sunlight has not been studied yet. Furthermore, it is noteworthy that despite in a previous study demonstrated 100 % degradation of ATZ using Fe-allophane catalyst after 24 and 8 h of reaction time through the heterogeneous Fenton and electro-Fenton processes, respectively [40]. The use of Fe–TiO$_2$-allophane catalysts to degrade ATZ through the heterogeneous dual-effect process represents a promissory opportunity to degrade ATZ in more friendly conditions (under sunlight) and with shorter reaction times.

Therefore, in this study, Fe–TiO$_2$-allophane catalysts with 6.0 % w/w of iron oxide and two different proportions of TiO$_2$ (10 % and 30 % w/w) were synthesized for the first time using an acid hydrolysis method. The catalytic performance of these catalysts was subsequently compared with TiO$_2$-allophane and Fe-allophane counterparts. These catalysts were characterized using scanning electron microscopy, X-ray diffraction, Fourier transform infrared spectra, diffusive reflectance spectra, and N$_2$ adsorption-desorption

Table 1

Nomenclature of prepared catalysts with different proportions of iron and/or titanium dioxide.

Nomenclature	Catalysts compositions
Allophane	Allophane clay
Fe-allophane	Allophane with 6.0 % w/w of iron oxide
10%TiO$_2$-allophane	Allophane with 10 % w/w of titanium dioxide
30%TiO$_2$-allophane	Allophane with 30 % w/w of titanium dioxide
Fe–10%TiO$_2$-allophane	Allophane with 6.0 % w/w of iron oxide and 10 % w/w of titanium dioxide
Fe–30%TiO$_2$-allophane	Allophane with 6.0 % w/w of iron oxide and 30 % w/w of titanium dioxide

isotherms. The catalytic performance of the different catalysts was evaluated in both photocatalysis (PC) and heterogeneous dual-effect (HDE) processes for atrazine degradation under natural sunlight. The study also examined the degradation of ATZ by HDE under artificial UV radiation. The influence of initial pH on ATZ degradation through the HDE process under sunlight was also conducted.

2. Experimental section

2.1. Chemicals

Atrazine (1-chloro-3-ethylamino-5-isopropylamino-2,4,6-triazine, PESTANAL, analytical standard), iron (III) nitrate nonahydrate (Fe(NO$_3$)$_3$·9H$_2$O, >98 %) and titanium tetrachloride for synthesis (TiCl$_4$, ≥97 %) were purchased from Sigma–Aldrich. Hydrochloride acid (HCl, 37 %), sulfuric acid (H$_2$SO$_4$, 97 %), sodium hydroxide (NaOH, ≥99 %), hydrogen peroxide for analysis (H$_2$O$_2$, 30 % w/w), ammonium acetate (CH$_3$CO$_2$NH$_4$, ≥99 %), acetonitrile (gradient grade for liquid chromatography, LiChrosolv®) and water (LC-MS grade) were supplied by Merck.

2.2. Synthesis of allophane and Fe-allophane

Allophane clay with a theoretical Si/Al ratio of 3.0 and a structure similar to that of hydrous feldspathoids was synthesized by coprecipitation of aluminum chloride and potassium silicate, as previously reported [38]. Allophane clay was impregnated with 6.0 % w/w iron oxide using a wet impregnation method with Fe(NO$_3$)$_3$·9H$_2$O as the iron source. The physical and chemical properties of these compounds were reported in a previous work [38].

2.3. Preparation of Fe–TiO$_2$-allophane and TiO$_2$-allophane catalysts

Fe–TiO$_2$-allophane catalysts were prepared by a simultaneous impregnation of iron oxide and TiO$_2$ by hydrolysis of titanium tetrachloride using a method adapted for allophane [42–44]. These catalysts were prepared with a fixed iron content of 6.0 % w/w, as was previously reported [38], and two proportions of TiO$_2$ (10 % and 30 % w/w). The nomenclature assigned to the synthesized catalysts is presented in Table 1. In brief, 2.0 g of allophane clay was mixed with 60 mL of distilled water and heated to 70 °C. Subsequently, the required amount of iron oxide was added as Fe(NO$_3$)$_3$·9H$_2$O simultaneously with dropwise TiCl$_4$ solution, maintaining the pH of the suspension at pH 2.5 by the addition of 1.0 M NaOH. The system was vigorously stirred for 4 h at 70 °C, followed by an additional 12 h at room temperature. The resulting dispersion underwent centrifugation and was repeatedly washed with distilled water until chloride ions were undetectable in the supernatant solution. Chloride detection was carried out by adding drops of 0.1 M AgNO$_3$, which form a precipitate in the presence of chloride. Finally, the samples were dried at 105 °C for 2 h and calcined at 450 °C for 4 h. The same procedure described above was used to prepare TiO$_2$-allophane catalysts with different proportions of TiO$_2$ (10 % and 30 % w/w) but without the addition of iron oxide.

2.4. Catalysts characterization

The morphologies of the catalysts were determined by scanning electron microscopy (SEM) using SU3500 HITACHI-Japan equipment. For SEM analysis, the samples were suspended in analytical grade methanol and sonicated for 5 min at 50 kW before being coated with gold palladium. Images were obtained at 18 keV and a magnification of 50000X. The crystalline phases of the catalysts were analyzed by powder X-ray diffraction (XRD) performed on a Bruker Endeavor diffractometer (Model D4/MAX-B, Billerica, MA, USA). Patterns were obtained using CuKα radiation at 40 kV and 20 mA in the 2Θ value range of 10–80° with a 0.02° step and counting time of 1 s. Fourier transform infrared spectra (FTIR) were recorded on an ALPHA FTIR-ATR Bruke spectrometer over a wavenumber range of 400–4000 cm^{-1}. The textural properties of the photocatalysts were determined by N$_2$ adsorption-desorption isotherms at 77 K using 3-FLEX Micromeritics equipment. Before the analysis, the samples were degassed for 6 h at 77 K using a SmartVacPrep device. The Brunauer, Emmett, and Teller (BET) method [45] was employed to calculate the specific surface area, while the pore size distribution was determined using the Barrett-Joyner-Halenda (BJH) method [46], with the total pore volume resulting from the adsorbed quantity at a p/p^o of 0.99. The chemical composition of the catalysts was determined by acid digestion according to the Bernas method [47,48]. The iron and titanium concentrations were determined by inductively coupled
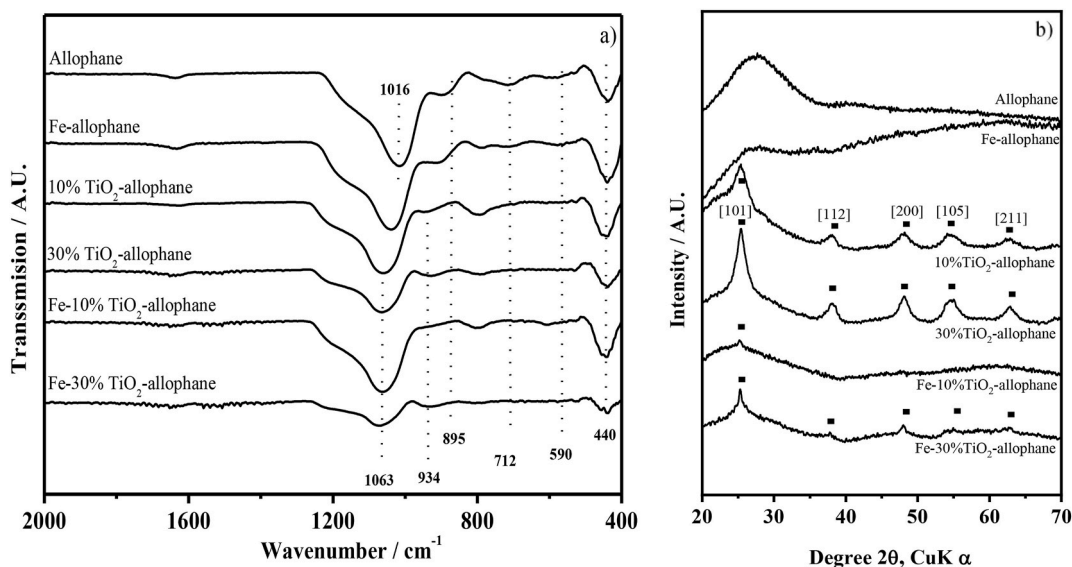
Fig. 1. FTIR spectra (a) and X-ray diffraction patterns (b) of allophane clays and allophane modified with iron and/or titanium dioxide.

plasma−optical emission spectrometry (ICP−OES) using a PerkinElmer, model OPTIMAN0770793. The light absorption of the catalysts was determined by diffuse reflectance spectroscopy (DRS) using a UV–Vis scanning spectrophotometer (Shimadzu UV-2450, Japan) equipped with a diffuse reflectance accessory. A TiO$_2$ thin film was placed in the sample holder on an integrated sphere for the reflectance measurements. A "total white" PerkinElmer reference material was used as the reference. The band gap energies (E$_g$) of the photocatalysts were estimated by the Kubelka-Munk (K-M) function and the Tauc plot [49,50]. It is assumed that these Fe–TiO$_2$-allophane and TiO$_2$-allophane photocatalysts are indirect semiconductors due to the presence of the anatase phase [42]. The band gap was obtained by plotting $(\alpha h\nu)^{1/2}$ vs. $h\nu$, giving rise to a straight line whose extrapolation to the x-axis provides the band gap value [51].

2.5. Atrazine degradation through photocatalysis

ATZ oxidation through photocatalysis (PC) was performed in a lab-scale photoreactor using a batch quartz reactor (0.2 L), equipped with a magnetic stirrer and constant airflow. The reactions were performed in the presence of natural sunlight irradiation. All sunlight tests started at 11:00 a.m. local time during the summer months of December and January and were conducted at the Universidad de la Frontera, Temuco, Chile (latitude: 38.4448°S, longitude 72.3650°W). The reactor was loaded with 100 mL of ATZ solution (10 mg L^{-1}) and 1.0 g L^{-1} catalyst dosage. ATZ degradation was assessed after 30 min in the dark to achieve adsorption equilibrium, followed by the initiation of photocatalytic reaction by exposing the reactor to sunlight. All experiments were performed under room conditions for 360 min at an initial pH of 3.0. During the reactions, at specified time intervals, a 1.0 mL sample of ATZ solution was withdrawn from the reactor and immediately filtered (0.2 μm) to determine the ATZ concentration using high-performance liquid chromatography (HPLC).

2.6. Atrazine degradation by heterogeneous dual-effect processes

ATZ oxidation through the heterogeneous dual-effect (HDE) process was carried out under the previously mentioned experimental conditions, alongside the addition of 240 μL of H$_2$O$_2$ (30 % w/w). ATZ degradation by HDE processes was also studied under artificial UV radiation using an aluminum UV chamber with 6 UV-A tubes of 8 W each (λ of 365 nm) positioned in front of the quartz reactor. The experimental conditions for ATZ degradation under UV radiation were the same as those described above for HDE processes under natural sunlight. The effect of the initial pH was investigated by studying ATZ degradation through the HDE process under sunlight at initial pH values of 3.0 and 5.0, as well as under auto-regulated pH conditions (6.3).

The chemical stability of iron oxide supported in the catalysts was studied by determining the concentration of iron in the solution (iron leaching) after the end of the catalytic reactions. The influence of H$_2$O$_2$ on ATZ degradation was determined under identical experimental conditions, omitting the addition of a catalyst (referred to as the blank sample).

2.7. Analytical methods

ATZ decay concentration was followed by HPLC MD-4015 Jasco LC-NET/ADC equipment provided with an array diode detector at 220 nm using a reverse-phase column RP18e (5 μm), according to the method previously described [38]. Thus, 40 % acetonitrile and

Table 2

Chemical composition, textural properties and band gap values of allophane clays and prepared catalysts of allophane with iron and/or titanium dioxide determined by ICP-OES, N_2 adsorption-desorption isotherm and diffuse reflectance spectra from Tauc plots, respectively.

Catalysts	Chemical composition (wt. %)					Textural properties			Band gap (E_g) (eV)
	Ti	Fe	Si	Al	Si/Al	BET surface area (m^2g^{-1})	Pore Volume (cm^3g^{-1})	Pore size (nm)	
Allophane	–	–	15.8	4.69	3.37	147	0.418	10.6	–
Fe-allophane	–	5.0	25.3	6.13	4.13	135	0.520	14.5	1.71
10%TiO$_2$-allophane	13.7	–	26.0	3.60	7.22	256	0.572	8.57	3.29
30%TiO$_2$-allophane	23.8	–	19.8	3.90	5.08	577	0.925	6.41	3.24
Fe–10%TiO$_2$-allophane	9.34	5.8	19.4	5.60	3.46	240	0.585	9.27	2.22
Fe–30%TiO$_2$-allophane	20.1	4.2	17.1	3.40	5.03	227	0.360	6.40	2.35

60 % ammonium acetate (0.1 mM) were used as mobile phases at 1.0 mL min^{-1} and 30 °C. The chemical oxygen demand (COD) at the beginning and end of the reactions was measured with a COD analyzer (HANNA HI83099). The iron leaching was determined by atomic adsorption analysis at the end of the catalytic reactions using a Thermo Scientific ICE 3000 Series.

3. Results and discussion

3.1. Catalysts characterization

FTIR-ATR spectrum of allophane clay (Fig. 1a) shows the characteristic bands of hydrous feldspathoid allophane. These bands appear at 440 cm^1, 712 cm^{-1}, and 1016 cm^{-1}, associated with the tetrahedral aluminosilicate framework. The peak observed at 590 cm^{-1} corresponds to octahedral aluminum, while the presence of Si–OH groups has been associated with the shoulder observed at 895 cm^{-1} [34,35,39]. Thus, as previously reported, hydrous feldspathoid allophane is composed of an outer polymerized Si tetrahedral sheet that forms the framework, with partial substitution of Al for Si. Meanwhile, the inner part is comprised of an incomplete Al sheet in an octahedral position [38]. In the presence of both iron and/or titanium oxides on the allophane structure, the peaks of the tetrahedral aluminosilicate framework are weakened or shifted to higher wavenumbers. For the catalyst containing iron oxide, this effect is attributed to the covalent bond formation between Si–O$^-$ groups of allophane clays and iron hydroxyl species in solution (Fe(OH)$^+$, Fe(OH)$^{2+}$, Fe(OH)$^{3+}$), which occurs due to the generation of electrostatic attractions [38,48]. In TiO$_2$-allophane and Fe–TiO$_2$-allophane catalysts, the effect arises from the interaction of Ti^{+4} with Si–O groups. A new signal appears at 934 cm^{-1}, associated with the stretching vibration of Si–O–Ti groups, as reported in studies of zeolite, silica and, clay modified with titanium dioxide [52–54]. This band at 934 cm^{-1} intensifies with increasing TiO$_2$ percentage in the catalyst, whereas bands associated with tetrahedral aluminosilicate decrease. These findings can result from potential aluminum dissolution due to the acidic conditions employed in catalyst preparation, favoring the formation of Si–O–Ti bonds. Similar effects were noted by Ono and Katsumata [55], demonstrating that after acid treatment, allophane clay could lose its structure, evidenced by the disappearance of the bands associated with the tetrahedral aluminosilicate framework in the FTIR spectrum. However, in this case, complete aluminum dissolution did not occur as the bands at 1016 cm^{-1} did not disappear completely, indicating that the method used to prepare the catalysts did not significantly impact the framework of the allophane. The chemical composition determined by ICP−OES (Table 2) confirms the results obtained from FTIR analysis, indicating an increase in the Si/Al ratio in the catalysts modified with TiO$_2$ compared to unmodified allophane clay.

The XRD patterns (Fig. 1b) show broad lines centered at 2Θ values of 26° and 40°, characteristic of an allophane amorphous structure [34–36]. These bands are present in all catalysts but are narrower and better resolved, especially the signal at 26°. These results suggest that, despite the amorphous structure of allophane clay remaining after modification with iron and/or titanium dioxide, there is a higher degree of ordering. This is evident, especially since the anatase structure exhibits signals in the same region indicated by the squares (■) in Fig. 1b. In the case of the Fe-allophane and Fe–TiO$_2$-allophane catalysts, the signals for iron oxides are not observed, which is evidence of very small nanoparticles of iron oxide finely dispersed on the allophane clay [36,39,40]. For the TiO$_2$-allophane, anatase planes were observed (■) at 2Θ values of 25.3°, 38.2°, 48.1°, 54–55°, and 62,1°, associated with the (101), (112), (200), (105), and (211) planes of anatase, respectively [56,57]. The XRD peak intensity of anatase planes decreases for the Fe–TiO$_2$-allophane catalysts. The decrease in the diffraction peak of the 101 plane in anatase is attributed to the substitution of Ti^{4+} by Fe^{3+} ions in the crystal lattice of the anatase structure. This is due to the similarity in ionic radius between Fe^{3+} (0.645 A°) and Ti^{4+} (0.604 A°) [28,30,56,58]. Therefore, the incorporation of iron oxide into the Fe–TiO$_2$-allophane catalysts led to a reduction in the crystallinity of anatase [59].

In the SEM micrographs (Fig. 2) all the catalysts exhibit highly porous aggregated particles, in agreement with the unitary structure of allophane clays reported in previous studies [36,38,60]. Fig. 2 shows that particle agglomeration and particle size decreased as increased the proportion of TiO$_2$ in allophane clays. This finding agrees with the report by Nishikiori et al. [41,61], that showed that the presence of allophane can prevent the particle growth of TiO$_2$. These results align with the textural properties of the different prepared catalysts, as determined by N_2 adsorption-desorption isotherms (Table 2). The textural properties of allophane clays closely resemble those reported in previous studies for allophane clays with a hydrous feldspathoid structure [38]. The specific surface area of
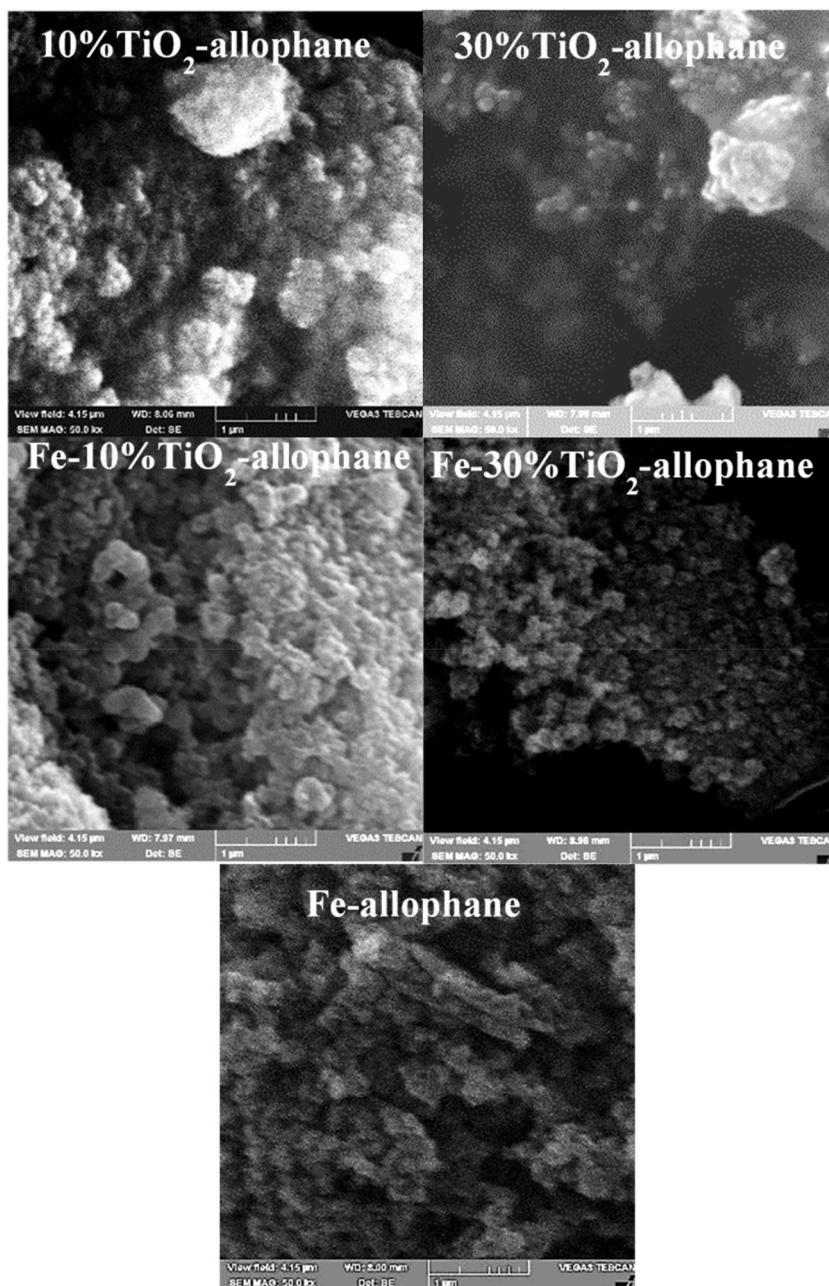
Fig. 2. Scanning electron microscopy of allophane clays modified with iron and/or titanium dioxide.

10%TiO_2-allophane and Fe–TiO_2-allophane catalysts increased almost double compared to the allophane clays, while the pore size decreased as the percentage of titanium dioxide on the catalysts increased. In the case of the 30%TiO_2-allophane, the results are surprising, as the specific surface area increased fourfold and the pore volume doubled compared to allophane clays. Furthermore, this catalyst exhibited the smallest pore size. These results have also been previously described for other clays; for example, Li et al. [62], reported an increase in the specific surface area of kaolinite-TiO_2 in comparison with kaolinite unmodified and pure TiO_2. The authors attributed this effect to the formation of small particles through oxide-support interactions to provide more active sites for enhanced catalytic activity and stability on the modified clay compared to the unmodified clays. These results agree with the FTIR and chemical composition analyses that show that more anatase nanoparticles are formed as the percentage of TiO_2 increases, forming new Ti–O–Si bonds attached to allophane clays. Additionally, the presence of iron oxide in the crystal lattice of TiO_2 in the Fe–TiO_2-allophane catalyst decreased the TiO_2 particle size, attributed to the inhibitory effect of Fe^{3+} on crystallization. This resulted in an enhancement of the specific surface area of the catalysts [58,59].
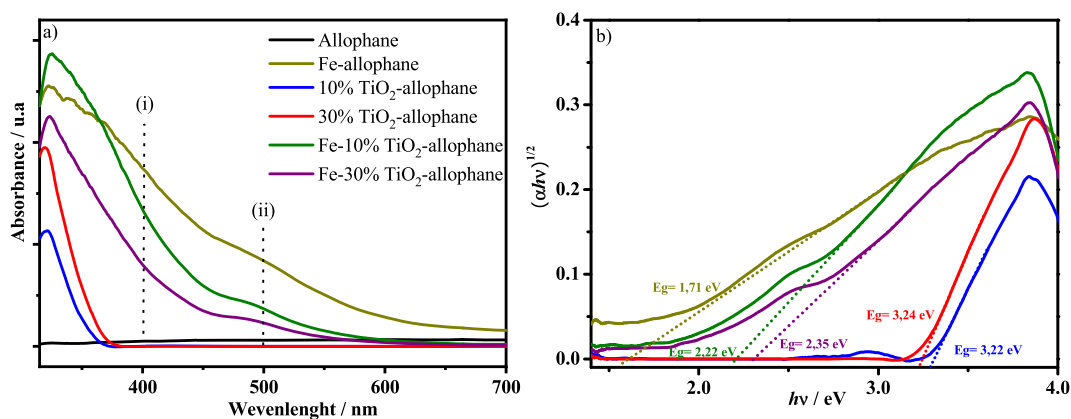
Fig. 3. UV-VIS diffuse reflectance spectra of the different prepared catalysts (a), and Tauc plot obtained by the indirect band gap (b).
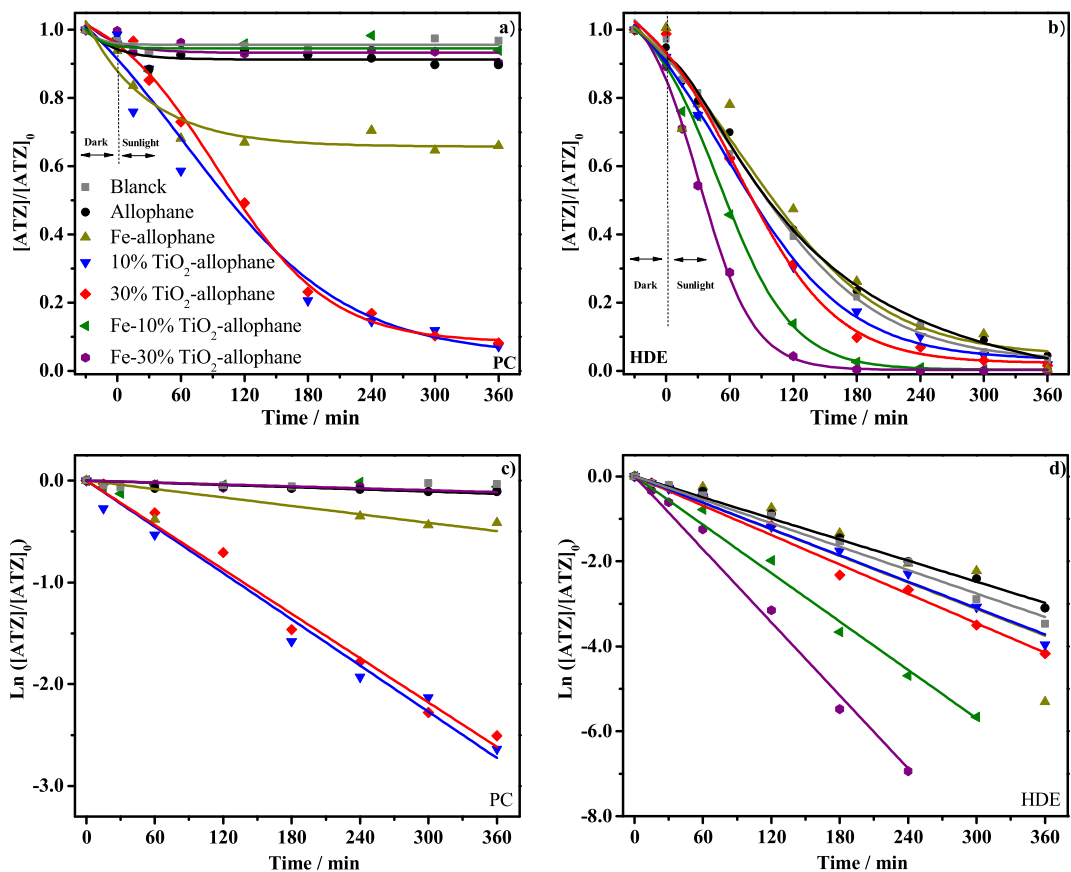
Fig. 4. Degradation of 10 mg L^{-1} of atrazine (a and b) and fitting of experimental data to the pseudo-first-order kinetic model (c and d) using 1.0 g L^{-1} of allophane clays and allophane modified with iron and/or of titanium dioxide through photocatalysis (PC) and the heterogeneous dual-effect process (HDE) at initial pH 3.0 and natural sunlight.

In the case of adding only iron oxide (Fe-allophane catalyst), both specific surface area and pore volume remain almost constant in comparison with parental allophane, showing an increase in the particle diameter, in agreement with previous works [38]. Thus, the prepared catalysts of TiO_2-allophane and Fe–TiO_2-allophane exhibit a positive influence on the catalytic surface area and, consequently, on photocatalytic activity, as will be discussed in the following. It has been widely reported that one of the main factors affecting photocatalytic performance is the surface area of the photocatalysts [58,59]. On the other hand, all catalysts present N_2 adsorption-desorption isotherm type IV (Fig. S1, supplementary material). At high relative pressures from 0.40 to 0.95, the isotherms exhibit hysteresis loops of type H3 corresponding to mesoporous adsorbent material (2–50 nm) [30].

The UV–vis diffuse reflectance spectra (DRS) of allophane clays and the different prepared catalysts are present in Fig. 3a. The allophane clays exhibit no signs of light absorption in both the UV and visible ranges. The absorption spectra of TiO_2-allophane catalysts show the characteristic absorption of TiO_2 band in the UV region with a band edge at 320 nm [30]. The intensity of this band increases with the percentage of TiO_2 in the sample, consistent with the higher content of anatase structure. After being supported with iron oxide, the photo response range of the Fe–TiO_2-allophane catalysts expanded to the visible light region. It is shown that the incorporation of iron oxide on TiO_2-allophane catalysts does not modify the position of the valence band edge of the TiO_2, as it remains similar to the TiO_2-allophane catalyst. However, new energy levels (Fe^{3+}/Fe^{4+}) of the transition Fe ions into the band gap of TiO_2 were introduced [59]. Consequently, for the Fe–TiO_2-allophane, the broad absorption band ranges centered at 400 nm can be attributed to the excitation of 3d electron of Fe^{3+} to the TiO_2 conduction band (charge transfer transition). On the other side, the band centered at 500 nm can be ascribed to the d-d transition of Fe^{3+} or the charge transfer transition between interacting iron ions (Fe^{3+} + Fe^{3+} → Fe^{4+} + Fe^{2+}) [63–65]. Therefore, a decrease in the energy band of Fe–TiO_2-allophane catalysts is expected. To validate this assumption, Fig. 3b and Table 2 present the Tauc-plot patterns of the different catalysts and the calculated band gap values, respectively. The Fe-allophane catalyst band gap was 1.71 eV, which is similar to the value reported for ferrihydrite [66]. Concerning the TiO_2-allophane catalysts, band gap values between 3.24 eV and 3.29 eV were obtained, which are typical of anatase structures [42, 67]. As expected, in the presence of iron oxide, the band gap values were reduced, obtaining very similar band gap values for both studied catalysts (Table 2).

3.2. Atrazine degradation by photocatalysis and heterogeneous dual-effect processes

Fig. 4 shows the degradation of ATZ through photocatalysis (PC) and heterogeneous dual-effect (HDE) processes under natural sunlight. In the case of the PC process (Fig. 4a), the degradation of ATZ in the presence of sunlight alone (blank sample) was minimal, approximately 3 %. This result was expected since the half-life for ATZ direct photolysis under natural sunlight ranges from 42.5 to 96 days, duration exceeding the reaction time (360 min) employed in this study [68,69]. Similarly, no ATZ degradation occurred in the PC process when unmodified allophane was used as the catalyst because allophane cannot exhibit photocatalytic activity under UV or visible light as was determined by UV–Vis-DR analysis. As depicted in Fig. 4a, degradation of ATZ occurs only in the first 30 min under dark conditions, attributed to the adsorption of ATZ on the allophane surface. Subsequently, under sunlight, the system stabilized and remained constant, achieving a 13 % removal of ATZ at the end of the 360 min of operation.

In a similar manner, Fe–TiO_2-allophane catalysts with 10 % and 30 % w/w TiO_2 exhibited low ATZ degradation values of 6 % and 10 %, respectively. It is evident that, regardless of the TiO_2 content, the presence of iron oxides on Fe–TiO_2-allophane catalysts inhibits the photocatalysis process under sunlight, resulting in similar ATZ degradation as observed with unmodified allophane clays. These results are unexpected, as the substitution of Ti^{4+} by Fe^{3+} ions in the crystal lattice of the anatase structure decreased the bandgap and improved the surface area of these catalysts. Consequently, it was expected that the presence of Fe^{3+} in the TiO_2 crystal lattice of the Fe–TiO_2-allophane catalysts would decrease the electron/hole recombination rate during the PC process under sunlight. However, it is possible that, due to the amount of iron loaded on the catalysts (6.0 % w/w), the iron was not fully incorporated into the crystal lattice, and the excess precipitated on the surface of allophane clays, forming small particles of iron oxide [40]. This could act as a recombination center for electrons and holes at the interface, preventing the charge carriers from reaching the surface and reacting with the adsorbed water and oxygen molecules [58,59].

In the case of Fe-allophane catalyst, 34 % of ATZ degradation was achieved in the PC process after 360 min of reaction time, due to the photocatalytic properties of iron oxide present in the allophane structure. As highlighted earlier, the Fe-allophane catalyst displays a poorly ordered iron oxide phase, similar to the ferrihydrite-like materials [13,38], reported as a semiconductor material able to oxide pollutants under sunlight [66]. This result agrees with the previously discussed band-gap value (1.71 eV) and the ability of Fe-allophane to adsorb the light across a broad wavelength range.

In contrast, the highest ATZ degradation in the PC process under sunlight was attained using TiO_2-allophane catalysts with 10 % and 30 % w/w of TiO_2, achieving nearly 90 % ATZ degradation. These results agree with the higher specific surface area exhibited by these catalysts compared to the parental allophane clays. This is attributed to the earlier discussed formation of small particles of anatase on the allophane surface, which provides more active sites for the photocatalytic degradation of ATZ. This phenomenon is favored by the reduction of particle agglomeration facilitated by the presence of allophane clays. The enhancement in ATZ degradation observed with TiO_2-allophane catalysts can be associated with the generation of radical species through the PC process, facilitated by the UV component of sunlight. This process initiates with the illumination of the TiO_2-allophane catalysts by light energy greater than their bandgap energy, leading to the production of electron-hole pairs (Eq. (1)). These charged carriers can either recombine or react with chemical species such as water or oxygen molecules to produce hydroxyl radicals and superoxide radical anions, respectively (Eqs. (2) and (3)). Moreover, hydroperoxyl radicals are formed through electron transfer from TiO_2 present in the catalyst structure to molecular oxygen, followed by consecutive protonation (Eq. (4)) [32,42,57].

$$TiO_2 + h\nu \rightarrow e^- + h^+ \qquad (1)$$

$$h^+ + H_2O \rightarrow H^+ + \bullet OH \qquad (2)$$

$$e^- + O_2 \rightarrow O_2^- \bullet \qquad (3)$$

$$e^- + O_2 + H^+ \rightarrow HO_2^\bullet \qquad (4)$$
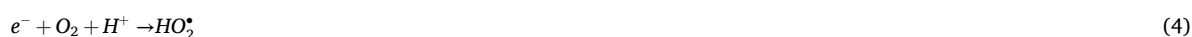
Table 3
ATZ degradation, chemical oxygen demand (COD) decay and kinetics parameters using the different catalysts with photocatalysis (PC) and heterogeneous dual-effect (HDE) processes at initial pH of 3.0 and under natural sunlight.

Catalyst	ATZ degradation %		COD decay %		Kinetics parameters			
					PC		HDE	
	PC	HDE	PC	HDE	k_1 min^{-1}	R^2	k_1 min^{-1}	R^2
Blank	3	96	n.v.[a]	n.v.[a]	n.a.[b]	n.a.[b]	0.00920	0.994
Allophane	13	95	n.v.[a]	n.v.[a]	0.000361	0.901	0.00827	0.997
Fe-allophane	34	98	n.v.[a]	22	0.001380	0.807	0.01041	0.882
10%TiO$_2$-allophane	92	99	25	53	0.007570	0.993	0.01033	0.996
30%TiO$_2$-allophane	91	99	33	64	0.007260	0.994	0.01153	0.995
Fe–10%TiO$_2$-allophane	6	100	n.v.[a]	53	n.a.[b]	n.a.[b]	0.01899	0.994
Fe–30%TiO$_2$-allophane	10	100	n.v.[a]	85	0.000316	0.902	0.02866	0.994

[a] n.v: no variation.
[b] n.a: no adjusted.

Table 4
Effect of initial pH in ATZ degradation, chemical oxygen demand (COD), iron leaching, and kinetics parameter using Fe–30%TiO$_2$-allophane catalyst with heterogeneous dual-effect process under natural sunlight.

Initial pH	ATZ degradation %	COD Decay %	Iron content mgL^{-a}	Kinetics parameters	
				k_1 min^{-a}	R^b
3.0	100	85	0.001	0.02866	0.994
5.0	99	35	n.d.[b]	0.01347	0.993
Auto-regulated (6.3)	61	n.v[a]	n.d.[b]	0.00323	0.921

[a] n.v: no variation.
[b] n.d: no detected (low detection limit).

In the heterogeneous dual-effect (HDE) process (Fig. 4b), all catalysts exhibited enhanced ATZ degradation compared to the photocatalytic (PC) process (Fig. 4a), achieving over 95 % ATZ degradation for all catalysts, including the blank (conducted in the presence of H$_2$O$_2$ and sunlight). To validate these results in terms of kinetic parameters, the experimental data were fitted to a pseudo-first-order kinetics model according to Equations (5) and (6).

$$\frac{dC}{dt} = -kC \tag{5}$$

$$\ln\frac{C_t}{C_0} = -kt \tag{6}$$

Where C_t and C_0 represent the ATZ concentration at a given time t and the initial time (t = 0), respectively. The pseudo-first-order kinetic (k, min^{-1}) can be determined by plotting the linear dependence of the slope of Ln [C_t/C_o] against reaction time (t). According to the model, the pseudo-first-order reaction rates were determined (Fig. 4b and c) and tabulated in Table 3, along with the degradation of ATZ and the chemical oxygen demand (COD) efficiencies for the different processes (PC and HDE).

As observed in Fig. 4b and Table 3, the presence of H$_2$O$_2$ in the HDE process improves the ATZ degradation from 3 % to 96 % for the blank and from 13 % to 95 % for the unmodified allophane clays after 360 min of reaction time, respectively, in comparison with the PC process. Whereas the pseudo-first-order rate constant increased nearly 23 times when allophane was used as the catalyst.

For the Fe-allophane catalyst, catalytic efficiency increased from 34 % in the PC to 98 % in the HDE process. In this process, the iron oxide present on the Fe-allophane catalysts reacts with H$_2$O$_2$ to generate hydroxyl radicals according to Equations 7 and 8 through a heterogeneous Fenton process [38,40]. Furthermore, the presence of sunlight accelerates Fe^{2+} regeneration and produces additional hydroxyl radicals (Equations (9) and (10)) through a photo-Fenton process [70]. This result is further confirmed by the pseudo-first-order rate constant, which increased 7.5 times compared to the PC process.

$$Fe^{2+} + H_2O_2 \rightarrow Fe^{3+} + OH^- + \bullet OH \tag{7}$$

$$Fe^{3+} + H_2O_2 \rightarrow Fe^{2+} + HO_2^{\bullet} + H^+ \tag{8}$$

$$Fe(OH)^{2+} + h\nu \rightarrow Fe^{2+} + \bullet OH \tag{9}$$

$$Fe(OOCR)^{2+} + h\nu \rightarrow Fe^{2+} + CO_2 + R^{\bullet} \tag{10}$$

In the case of TiO_2-allophane catalysts, the improvement in ATZ degradation by the HDE process was smaller (approximately 8 %), whereas the pseudo-first-order rate constants were slightly higher (nearly 1.4 times higher than the PC process) due to the addition of H_2O_2 into the HDE process.

As expected, Fe–TiO_2-allophane catalysts exhibited the highest ATZ oxidation under sunlight in the HDE process. With values of 100 % ATZ oxidation for both Fe–TiO_2-allophane catalysts, the results are largely higher than the value of nearly 10 % ATZ degradation obtained by PC. Additionally, the pseudo-first order-rate constant was significantly higher than the value determined by the PC process (see Table 4).

It is important to note that, despite all catalysts showing high ATZ degradation efficiencies in the HDE process (Fig. 4b), the time required to achieve almost complete ATZ degradation varied depending on the catalyst used. In the case of Fe–TiO_2.allophane catalysts, the reaction time necessary to achieve 100 % ATZ oxidation decreased as the percentage of TiO_2 on the Fe–TiO_2-allophane catalysts increased, being the pseudo-first-order rate constant of Fe–30%TiO_2-allophane catalyst 1.5 times higher than the value for Fe-10%TiO_2-allophane catalyst. Thus, with the Fe–30%TiO_2-allophane catalyst, it was possible to achieve 100 % ATZ oxidation in 180 min of reaction time, whereas in the case of Fe–10%TiO_2-allophane, 100 % ATZ oxidation was obtained after 4 h reaction time. Similarly, in the case of TiO_2-allophane catalysts, the pseudo-first-order reaction rates were lower than those of the Fe–TiO_2-allophane catalysts. Therefore, to achieve a similar percentage in ATZ degradation (99 %), reaction times of approximately 360 min were necessary. These results indicate that in the HDE process performed under natural sunlight, ATZ is degraded in shorter times using Fe–TiO_2-allophane compared to TiO_2-allophane or Fe-allophane catalysts. These results agree with the reported synergetic effect in the heterogeneous dual-effect process due to the simultaneous presence of iron oxide and titanium dioxide on the catalyst [19,20,57,71]. Similar findings were also reported by Yang et al. [72], who achieved a 95 % ATZ degradation rate after 30 min of reaction time using a Fe–TiO_2 catalyst under visible light. Furthermore, these results represent a significant improvement compared to a previous study on ATZ degradation using Fe-allophane catalyst, where similar degradation rates were achieved but required reaction time of 24 and 8 h in the heterogeneous Fenton and electro-Fenton processes, respectively [40].

The observed synergetic effect of the Fe–TiO_2-allophane catalyst in ATZ degradation under sunlight and H_2O_2 can be attributed to a reduction in the electron/hole recombination rate, resulting in an enhanced catalytic efficiency when compared to the condition where the processes are separated (using Fe-allophane or TiO_2-allophane catalysts). This is because Fe^{3+}, incorporated into the TiO_2 crystal lattice of the Fe–TiO_2-allophane catalysts, captures the electrons generated on the TiO_2 surface and participates in the regeneration of Fe^{2+} ions according to Equation (11) [19,20,25,73]. Simultaneously, the iron oxide present on the catalysts of Fe–TiO_2-allophane generates hydroxyl radicals through the reaction with H_2O_2, as described above by a Fenton-based process (Eqs. (7) and (8)), plus a photo Fenton process (Eqs. (9) and (10)) mediated by sunlight [16,32].

$$Fe^{3+} + e^- \rightarrow Fe^{2+}(electron\ trap) \tag{11}$$

It is also important to remark that the reduction of the band gap of the Fe–TiO_2-allophane catalyst allows for extending the absorption light range into the visible light spectrum, as determined by UV–Vis-DRS analysis. In this way, in this work was possible to degrade ATZ under more environmentally friendly conditions, using sunlight as the light source [74]. This assumption was confirmed by studying the ATZ degradation through the HDE process under artificial UV light (performed at 365 nm). The results show that the ATZ degradation efficiencies range from 20 % to 65 % after 360 min of reaction time, depending on the catalyst used to perform the reaction (see Fig. S2 and Table S1 of supplementary material). Under sunlight, there is a contribution of both UV radiation (including UV-A and UV-B) and visible light, enhancing atrazine removal compared to artificial UV radiation. In the case of the catalyst of Fe-allophane, its band gap (1.71 eV) allows absorbed energy in visible light; therefore, it is expected that the photo-Fenton process is more efficient under solar light than artificial UV light [75].

The good performance of the HDE process under sunlight using the catalysts of Fe–TiO_2-allophane was also confirmed by determining the chemical oxygen demand (COD), which represents the amount of oxygen (mg) necessary for all the organic compounds present in 1 L of solution to be mineralized [19,42]. As shown in Table 3, the HDE process achieves higher mineralization efficiencies than the PC process. This shows that the mineralization efficiency improves with the percentage of TiO_2 on the Fe–TiO_2-allophane catalysts. Thus, the highest mineralization efficiency (85 %) was obtained with the catalyst with a higher percentage of TiO_2. This COD decay value is an important result because it is higher than the range between 10 and 30 % reported by other authors for ATZ mineralization using PC processes [76–78]. As has been widely reported, ATZ mineralization is difficult because ATZ is transformed into intermediate products, with cyanuric acid being the ultimate degradation product, which is a highly stable and persistent compound [11,69]. Therefore, these results suggest that the Fe–30%TiO_2-allophane catalyst could mineralize cyanuric acid by the HDE process under sunlight.

3.3. Effect of pH on atrazine oxidation by HDE process

The pH of the reaction can play an important role in the effectiveness of a given catalyst under a Fenton-like reaction [13] or photocatalytic processes [79]. In addition, for a friendlier wastewater treatment technology, it is preferable to degrade the organic pollutants at auto-regulated pH or under the less possible acidic conditions to avoid the excessive use of acid for maintaining the pH of the reaction. In addition, the leaching of iron from the catalyst could occur under acidic conditions [13,39]. For these reasons, was also studied ATZ degradation by the HDE process at auto-regulated pH (initial pH 6.3), slightly acidic conditions (initial pH 5.0), and acidic conditions (pH 3.0) using the best catalyst determined above. As shown in Fig. 5, ATZ degradation increased as the initial pH decreased, with a pseudo-first-order reaction rate 2 times higher for the reaction performed at an initial pH of 3.0 than the initial pH of
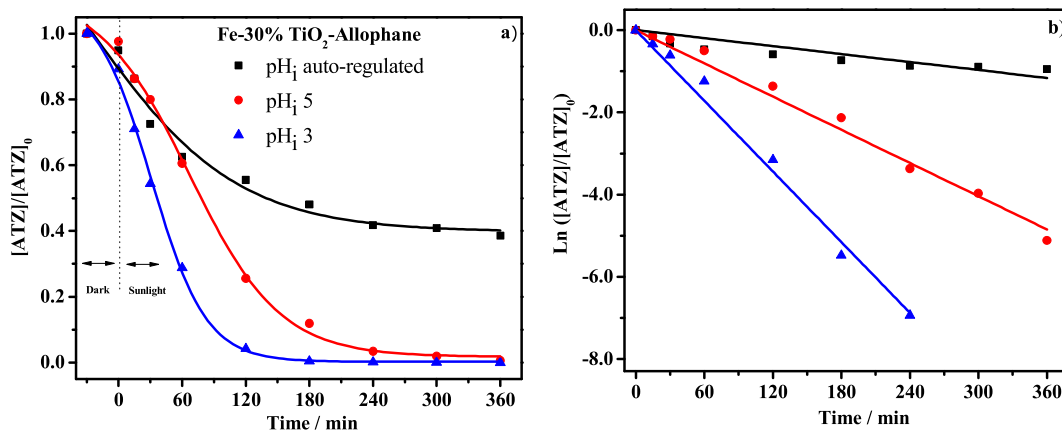
Fig. 5. Influence of initial pH on 10 mg L^{-1} atrazine degradation through the heterogeneous dual-effect process using 1.0 mg L^{-1} Fe–30%TiO_2-allophane catalyst under sunlight (a) including the corresponding plot according to the pseudo-first-order kinetic model (b).

5.0 and almost 9 times higher than autoregulated pH (Table 4). While the optimum pH reported for the Fenton process is typically around pH 3.0 [80,81], it is noteworthy that under less acidic conditions (initial pH 5.0), complete removal of ATZ was achievable. However, this accomplishment necessitated an extended reaction time of 6 h and resulted in a COD decay of 35 %, in contrast to the 85 % ATZ degradation observed at pH 3.0. Similar results have been reported using Fe–TiO_2 clay catalysts for degrading organic pollutants, showing catalytic activity at pH values between 4.0 and 5.0 [42,82]. In addition, at an initial pH of 5.0 and auto-regulated pH, no leaching of iron was observed (Table 4), whereas, at an initial pH of 3.0, the leaching of iron was minimal (0.001 mg L^{-1}). The results show the high stability of the Fe–TiO_2-allophane catalysts and confirm that with these catalysts, the dual-effect process occurs in a heterogeneous phase. This is the opposite of the dual effect process proposed in the literature, where the process is favored by the soluble iron species from catalyst leaching [17,18,20,71].

4. Conclusions

In this study, we propose for the first time, the utilization of Fe–TiO_2-allophane catalysts with 6.0 % w/w of iron oxide and two different proportions of TiO_2 (10 % and 30 % w/w) for atrazine (ATZ) degradation through the heterogeneous dual-effect (HDE) process under sunlight. Comparative analyses with Fe-allophane and TiO_2-allophane catalysts were conducted in both photocatalysis (PC) and HDE processes. FTIR spectra of the prepared catalysts reveal the characteristic hydrous feldspathoid structure of allophane, confirming the formation of new bonds between Si–O groups of allophane clays and iron hydroxyl species, as well as new Si–*O*–Ti bonds that increased with higher TiO_2 content. The TiO_2 in all catalysts exhibited an anatase structure, increasing with the higher proportions of TiO_2 on allophane clays. Iron oxide in the Fe–TiO_2-allophane catalyst was incorporated through the substitution of Ti^{4+} by Fe^{3+} ions in the crystal lattice of the anatase structure and by precipitation on the surface of allophane clays, forming small particles of iron oxide. Both the presence of allophane clays and iron oxide in the crystal lattice of TiO_2 decreased the agglomeration and particle size of TiO_2, resulting in an enhanced specific surface area and pore volume for all catalysts. Additionally, the incorporation of iron oxide reduced the band gap of the Fe–TiO_2-allophane catalysts, expanding their photoresponse to visible light. In the PC process, the highest ATZ degradation was achieved with the TiO_2-allophane catalysts, achieving nearly 90 % ATZ degradation, attributed to the generation of radical species through the PC process facilitated by the UV component of sunlight. Different proportions of TiO_2 on TiO_2-allophane catalysts did not significantly influence ATZ degradation through the PC process, obtaining similar degradation efficiencies and pseudo-first-order reaction rates for both catalysts. In contrast, in the HDE process, Fe–TiO_2 allophane catalysts demonstrated synergetic effects in ATZ degradation under sunlight compared to the separated processes (using Fe-allophane or TiO_2-allophane catalysts). Additionally, under sunlight, a higher proportion of TiO_2 on Fe–TiO_2-allophane catalysts resulted in a faster time to achieve 100 % ATZ degradation. Thus, Fe–30%TiO_2-allophane catalysts exhibited superior ATZ degradation and COD removal. The HDE process was also performed under less acidic conditions (initial pH 5.0), achieving complete ATZ degradation after 6 h without iron leaching. Consequently, in this work, Fe–TiO_2-allophane catalysts are presented as a promising alternative to contribute to the reduction of emerging pollutants from wastewater under environmentally friendly conditions using the heterogeneous dual-effect process.

Data availability statement

Data will be made available on request.

CRediT authorship contribution statement

Jorge Castro-Rojas: Writing – review & editing, Writing – original draft, Methodology, Investigation, Funding acquisition, Formal analysis, Conceptualization. **Pablo Jofré-Dupre:** Methodology, Investigation. **Néstor Escalona:** Writing – review & editing, Methodology, Investigation. **Elodie Blanco:** Writing – review & editing, Methodology, Investigation. **María Soledad Ureta-Zañartu:** Writing – review & editing, Methodology, Investigation. **Maria Luz Mora:** Writing – review & editing, Supervision, Funding acquisition, Conceptualization. **Elizabeth Garrido-Ramírez:** Writing – review & editing, Writing – original draft, Supervision, Resources, Methodology, Conceptualization.

Declaration of competing interest

The authors declare the following financial interests/personal relationships which may be considered as potential competing interests:Elizabeth Garrido Ramirez reports financial support was provided by National Agency for Research and Development, Chile. Maria de la Luz Mora reports financial support was provided by National Agency for Research and Development, Chile. Jorge Castro-Rojas reports financial support was provided by National Agency for Research and Development, Chile. If there are other authors, they declare that they have no known competing financial interests or personal relationships that could have appeared to influence the work reported in this paper.

Acknowledgments

Appendix A. Supplementary data

Supplementary data to this article can be found online at https://doi.org/10.1016/j.heliyon.2024.e32894.

References

[1] H. Ramírez-Malule, D.H. Quiñones-Murillo, D. Manotas-Duque, Emerging contaminants as global environmental hazards. A bibliometric analysis, Emerg. Contam. 6 (2020) 179–193, https://doi.org/10.1016/j.emcon.2020.05.001.

[2] G. Reichert, S. Hilgert, S. Fuchs, J.C.R. Azevedo, Emerging contaminants and antibiotic resistance in the different environmental matrices of Latin America, Environ. Pollut. 255 (2019), https://doi.org/10.1016/j.envpol.2019.113140.

[3] M.C.O. Souza, B.A. Rocha, J.A. Adeyemi, M. Nadal, J.L. Domingo, F. Barbosa, Legacy and emerging pollutants in Latin America: a critical review of occurrence and levels in environmental and food samples, Sci. Total Environ. 848 (2022), https://doi.org/10.1016/j.scitotenv.2022.157774.

[4] C. Peña-Guzmán, S. Ulloa-Sánchez, K. Mora, R. Helena-Bustos, E. Lopez-Barrera, J. Alvarez, M. Rodriguez-Pinzón, Emerging pollutants in the urban water cycle in Latin America: a review of the current literature, J. Environ. Manage. 237 (2019) 408–423, https://doi.org/10.1016/j.jenvman.2019.02.100.

[5] M. Mofijur, M.M. Hasan, S.F. Ahmed, F. Djavanroodi, I.M.R. Fattah, A.S. Silitonga, M.A. Kalam, J.L. Zhou, T.M.Y. Khan, Advances in identifying and managing emerging contaminants in aquatic ecosystems: analytical approaches, toxicity assessment, transformation pathways, environmental fate, and remediation strategies, Environ. Pollut. 341 (2024) 122889, https://doi.org/10.1016/j.envpol.2023.122889.

[6] T. Deblonde, C. Cossu-Leguille, P. Hartemann, Emerging pollutants in wastewater: a review of the literature, Int. J. Hyg Environ. Health 214 (2011) 442–448, https://doi.org/10.1016/j.ijheh.2011.08.002.

[7] M. Triassi, P. Montuori, D.P. Provvisiero, E. De Rosa, F. Di Duca, P. Sarnacchiaro, S. Díez, Occurrence and spatial-temporal distribution of atrazine and its metabolites in the aquatic environment of the Volturno River estuary, southern Italy, Sci. Total Environ. 803 (2022), https://doi.org/10.1016/j.scitotenv.2021.149972.

[8] M.J. Climent, E. Herrero-Hernández, M.J. Sánchez-Martín, M.S. Rodríguez-Cruz, P. Pedreros, R. Urrutia, Residues of pesticides and some metabolites in dissolved and particulate phase in surface stream water of Cachapoal River basin, central Chile, Environ. Pollut. 251 (2019) 90–101, https://doi.org/10.1016/j.envpol.2019.04.117.

[9] B.S. Rathi, P.S. Kumar, P.L. Show, A review on effective removal of emerging contaminants from aquatic systems: current trends and scope for further research, J. Hazard Mater. 409 (2021) 124413, https://doi.org/10.1016/j.jhazmat.2020.124413.

[10] M. Kucka, K. Pogrmic-majkic, S. Fa, S.S. Stojilkovic, R. Kovacevic, Atrazine acts as an endocrine disrupter by inhibiting cAMP-speci fi c phosphodiesterase-4, Toxicol. Appl. Pharmacol. 265 (2012) 19–26, https://doi.org/10.1016/j.taap.2012.09.019.

[11] H. Jiang, C.A. Adams, Treatability of chloro-s-triazines by conventional drinking water treatment technologies, Water Res. 40 (2006) 1657–1667, https://doi.org/10.1016/j.watres.2006.02.013.

[12] A. Roberson, M. Mcguire, D. Khiari, M. Pirnie, M. Pirnie, S. Monica, Occurrence and removal of chloro-s-triazines in water treatment plants, Environ. Sci. Technol. 40 (2006) 3609–3616, https://doi.org/10.1002/j.1551-8833.2006.tb07782.x.

[13] E.G. Garrido-Ramírez, B.K.G. Theng, M.L. Mora, Clays and oxide minerals as catalysts and nanocatalysts in Fenton-like reactions - a review, Appl. Clay Sci. 47 (2010) 182–192, https://doi.org/10.1016/j.clay.2009.11.044.

[14] A.M. Méndez-Torres, J. Castro, F. Fernández, E. Garrido-Ramírez, N. Escalona, C. Gutiérrez, J.F. Marco, M. Soledad Ureta-Zañartu, Electrodes based on zeolites modified with cobalt and/or molybdenum for pesticide degradation. Part I: physicochemical characterization and efficiency of the electrodes for O2 reduction and H2O2 production, Electrocatalysis 10 (2019) 95–111, https://doi.org/10.1007/s12678-018-0500-4.

[15] J. Castro, F. Fernández, F. Olivares, C. Berríos, E. Garrido-Ramírez, E. Blanco, N. Escalona, A. Aspée, P. Barrías, M.S. Ureta-Zañartu, Electrodes based on zeolites modified with cobalt and/or molybdenum for pesticide degradation: part II—2,4,6-trichlorophenol degradation, J. Solid State Electrochem. 25 (2021) 117–131, https://doi.org/10.1007/s10008-020-04590-6.

[16] O. Fawzi Suleiman Khasawneh, P. Palaniandy, Removal of organic pollutants from water by Fe2O3/TiO2 based photocatalytic degradation: a review, Environ. Technol. Innov. 21 (2021) 101230, https://doi.org/10.1016/j.eti.2020.101230.

[17] K. Aggarwal, A. Verma, P. Bansal, A. Singh, Heterogeneous photo-Fenton and photocatalytic degradation studies of 2-chloro-4-nitrophenol (2Cl4NP) using foundry sand and TiO2 coated cement/clay beads, Brazilian J. Chem. Eng. 34 (2017) 747–758, https://doi.org/10.1590/0104-6632.20170343s2015070.

[18] P. Bansal, A. Verma, Synergistic effect of dual process (photocatalysis and photo-Fenton) for the degradation of Cephalexin using TiO2 immobilized novel clay beads with waste fly ash/foundry sand, J. Photochem. Photobiol. Chem. 342 (2017) 131–142, https://doi.org/10.1016/j.jphotochem.2017.04.010.

[19] P. Bansal, A. Verma, Novel Fe-TiO2 composite driven dual effect for reduction in treatment time of pentoxifylline: slurry to immobilized approach, Mater. Des. 125 (2017) 135–145, https://doi.org/10.1016/j.matdes.2017.03.083.

[20] P. Bansal, A. Verma, In-situ dual effect studies using novel Fe-TiO2 composite for the pilot-plant degradation of pentoxifylline, Chem. Eng. J. 332 (2018) 682–694, https://doi.org/10.1016/j.cej.2017.09.121.

[21] K. Fouad, M. Gar Alalm, M. Bassyouni, M.Y. Saleh, Optimization of catalytic wet peroxide oxidation of carbofuran by Ti-LaFeO3 dual photocatalyst, Environ. Technol. Innov. 23 (2021) 101778, https://doi.org/10.1016/j.eti.2021.101778.

[22] L.C. Almeida, B.F. Silva, M.V.B. Zanoni, Photoelectrocatalytic/photoelectro-Fenton coupling system using a nanostructured photoanode for the oxidation of a textile dye: kinetics study and oxidation pathway, Chemosphere 136 (2015) 63–71, https://doi.org/10.1016/j.chemosphere.2015.04.042.

[23] F.C. Moreira, V.J.P. Vilar, A.C.C. Ferreira, F.R.A. dos Santos, M. Dezotti, M.A. Sousa, C. Gonçalves, R.A.R. Boaventura, M.F. Alpendurada, Treatment of a pesticide-containing wastewater using combined biological and solar-driven AOPs at pilot scale, Chem. Eng. J. 209 (2012) 429–441, https://doi.org/10.1016/j.cej.2012.08.009.

[24] Y. Xie, C. Liu, D. Li, Y. Liu, Applied Surface Science in situ-generated H 2 O 2 with NCQDs/MIL-101 (Fe) by activating O 2 : a dual effect of photocatalysis and photo-Fenton for efficient removal of tetracyline at natural pH, Appl. Surf. Sci. 592 (2022) 153312, https://doi.org/10.1016/j.apsusc.2022.153312.

[25] I. Thakur, A. Verma, B. Örmeci, V. Sangal, Applications of waste-derived visibly active Fe-TiO2 composite incorporating the hybrid process of photocatalysis and photo-Fenton for the inactivation of E. coli, Environ. Sci. Pollut. Res. 29 (2022) 72247–72259, https://doi.org/10.1007/s11356-022-19202-1.

[26] H. Zangeneh, A.A.L. Zinatizadeh, M. Habibi, M. Akia, M. Hasnain Isa, Photocatalytic oxidation of organic dyes and pollutants in wastewater using different modified titanium dioxides: a comparative review, J. Ind. Eng. Chem. 26 (2015) 1–36, https://doi.org/10.1016/j.jiec.2014.10.043.

[27] Y. Cong, Z. Li, Y. Zhang, Q. Wang, Q. Xu, Synthesis of α-Fe 2O 3/TiO 2 nanotube arrays for photoelectro-Fenton degradation of phenol, Chem. Eng. J. 191 (2012) 356–363, https://doi.org/10.1016/j.cej.2012.03.031.

[28] B. Palanisamy, C.M. Babu, B. Sundaravel, S. Anandan, V. Murugesan, Sol – gel synthesis of mesoporous mixed Fe 2 O 3/TiO2 photocatalyst : application for degradation of 4-chlorophenol, J. Hazard Mater. 252–253 (2013) 233–242, https://doi.org/10.1016/j.jhazmat.2013.02.060.

[29] B. Szczepanik, Photocatalytic degradation of organic contaminants over clay-TiO2 nanocomposites: a review, Appl. Clay Sci. 141 (2017) 227–239, https://doi.org/10.1016/j.clay.2017.02.029.

[30] M. Zhou, J. Yu, B. Cheng, Effects of Fe-doping on the photocatalytic activity of mesoporous TiO 2 powders prepared by an ultrasonic method, J. Hazard Mater. 137 (2006) 1838–1847, https://doi.org/10.1016/j.jhazmat.2006.05.028.

[31] M. Aram, M. Farhadian, A.R. Solaimany Nazar, S. Tangestaninejad, P. Eskandari, B.H. Jeon, Metronidazole and Cephalexin degradation by using of Urea/TiO2/ ZnFe2O4/Clinoptiloite catalyst under visible-light irradiation and ozone injection, J. Mol. Liq. 304 (2020) 112764, https://doi.org/10.1016/j.molliq.2020.112764.

[32] S. Fan, S. Luo, Y. Wang, X. Yue, D. Zheng, Z. Zhang, X. Fu, W. Dai, TiO 2 -based Pd/Fe bimetallic modification for the efficient photothermal catalytic degradation of toluene : the synergistic effect of ● O – 2 and ● OH species, Sep. Purif. Technol. 336 (2024) 126256, https://doi.org/10.1016/j.seppur.2023.126256.

[33] L.R. do Santos, A.J.S. Mascarenhas, L.A. Silva, Preparation and evaluation of composite with a natural red clay and TiO2 for dye discoloration assisted by visible light, Appl. Clay Sci. 135 (2017) 603–610, https://doi.org/10.1016/j.clay.2016.11.002.

[34] S. Ohta, K. Yoshida, T. Hongo, Synthesis of allophane from rice husk ash and its use as a phosphate adsorbent: a novel approach, J. Environ. Chem. Eng. 10 (2022) 108634, https://doi.org/10.1016/j.jece.2022.108634.

[35] Y. Li, M. Camps-Arbestain, C.P. Whitby, T. Wang, C.W. Mueller, C. Hoeschen, M.H. Beare, Functional complexity explains the depth-dependent response of organic matter to liming at the nanometer scale, Geoderma 408 (2022) 115560, https://doi.org/10.1016/j.geoderma.2021.115560.

[36] P. Du, S. Wang, P. Yuan, J. Liu, D. Liu, H. Guo, X. Xiang, X. Guo, Structure of allophanes with varied Si/Al molar ratios and implications to their differentiation on Mars, Icarus 382 (2022) 115057, https://doi.org/10.1016/j.icarus.2022.115057.

[37] G. Mora, M.L. Escudey, M. Galindo, Síntesis y caracterización de suelos alofanicos, Soc. Chil. Quim. 39 (1994) 237–243.

[38] E.G. Garrido-Ramírez, M.V. Sivaiah, J. Barrault, S. Valange, B.K.G. Theng, M.S. Ureta-Zañartu, M.D.L.L. Mora, Catalytic wet peroxide oxidation of phenol over iron or copper oxide-supported allophane clay materials: influence of catalyst SiO 2/Al 2O 3 ratio, Microporous Mesoporous Mater. 162 (2012) 189–198, https://doi.org/10.1016/j.micromeso.2012.06.038.

[39] E.G. Garrido-Ramírez, J.F. Marco, N. Escalona, M.S. Ureta-Zañartu, Preparation and characterization of bimetallic Fe-Cu allophane nanoclays and their activity in the phenol oxidation by heterogeneous electro-Fenton reaction, Microporous Mesoporous Mater. 225 (2016) 303–311, https://doi.org/10.1016/j.micromeso.2016.01.013.

[40] E.G. Garrido-Ramírez, M.L. Mora, J.F. Marco, M.S. Ureta-Zañartu, Characterization of nanostructured allophane clays and their use as support of iron species in a heterogeneous electro-Fenton system, Appl. Clay Sci. 86 (2013) 153–161, https://doi.org/10.1016/j.clay.2013.10.001.

[41] H. Nishikiori, M. Furukawa, T. Fujii, Degradation of trichloroethylene using highly adsorptive allophane-TiO2 nanocomposite, Appl. Catal. B Environ. 102 (2011) 470–474, https://doi.org/10.1016/j.apcatb.2010.12.028.

[42] N. Davari, M. Farhadian, A.R.S. Nazar, M. Homayoonfal, Degradation of diphenhydramine by the photocatalysts of ZnO/Fe2O3 and TiO2/Fe2O3 based on clinoptilolite: structural and operational comparison, J. Environ. Chem. Eng. 5 (2017) 5707–5720, https://doi.org/10.1016/j.jece.2017.10.052.

[43] P. Eskandari, M. Farhadian, A.R. Solaimany Nazar, B.H. Jeon, Adsorption and photodegradation efficiency of TiO2/Fe2O3/PAC and TiO2/Fe2O3/zeolite nanophotocatalysts for the removal of cyanide, Ind. Eng. Chem. Res. 58 (2019) 2099–2112, https://doi.org/10.1021/acs.iecr.8b05073.

[44] C. Wang, Y. Li, Preparation and characterisation of S doped TiO2/natural zeolite with photocatalytic and adsorption activities, Mater. Technol. 29 (2014) 204–209, https://doi.org/10.1179/1753555714Y.0000000127.

[45] S. Brunauer, P.H. Emmett, E. Teller, Adsorption of gases in multimolecular layers, J. Am. Chem. Soc. 60 (1938) 309–319, https://doi.org/10.1021/ja01269a023.

[46] E.P. Barrett, L.G. Joyner, P.P. Halenda, The determination of pore volume and area distributions in porous substances. I. Computations from nitrogen isotherms, J. Am. Chem. Soc. 73 (1951) 373–380, https://doi.org/10.1021/ja01145a126.

[47] B. Bernasl, A New Method for Decomposition and Com P Re, 1968, p. 648.

[48] A.A. Jara, S. Goldberg, M.L. Mora, Studies of the surface charge of amorphous aluminosilicates using surface complexation models, J. Colloid Interface Sci. 292 (2005) 160–170, https://doi.org/10.1016/j.jcis.2005.05.083.

[49] A.J. Deotale, R.V. Nandedkar, Correlation between particle size, strain and band gap of iron oxide nanoparticles, Mater. Today Proceeding 3 (2016) 2069–2076, https://doi.org/10.1016/j.matpr.2016.04.110.

[50] J.F. Guayaquil-Sosa, B. Serrano-Rosales, P.J. Valadés-Pelayo, H. de Lasa, Photocatalytic hydrogen production using mesoporous TiO2 doped with Pt, Appl. Catal. B Environ. 211 (2017) 337–348, https://doi.org/10.1016/j.apcatb.2017.04.029.

[51] L. Yang, B. Kruse, Revised kubelka–munk theory I theory and application, J. Opt. Soc. Am. A 21 (2004) 1933, https://doi.org/10.1364/josaa.21.001933.

[52] H. Nishikiori, S. Matsunaga, M. Iwasaki, N. Zettsu, M. Yamakawa, A. Kikuchi, T. Yamakami, K. Teshima, Formation of silica nanolayer on titania surface by photocatalytic reaction, Appl. Catal. B Environ. 241 (2019) 299–304, https://doi.org/10.1016/j.apcatb.2018.09.046.

[53] D.I. Petkowicz, R. Brambilla, C. Radtke, C.D.S. da Silva, Z.N. da Rocha, S.B.C. Pergher, J.H.Z. dos Santos, Photodegradation of methylene blue by in situ generated titania supported on a NaA zeolite, Appl. Catal. Gen. 357 (2009) 125–134, https://doi.org/10.1016/j.apcata.2008.12.040.

[54] B.T. Djonse Justin, N. Blaise, H.G. Valery, Investigation of the photoactivation effect of TiO2 onto carbon-clay paste electrode by cyclic voltammetry analysis, Heliyon 9 (2023) e13474, https://doi.org/10.1016/j.heliyon.2023.e13474.

[55] Y. Ono, K. ichi Katsumata, Enhanced photocatalytic activity of titanium dioxide/allophane mixed powder by acid treatment, Appl. Clay Sci. 90 (2014) 61–66, https://doi.org/10.1016/j.clay.2013.12.018.

[56] Y. Cardona, A. Węgrzyn, P. Miśkowiec, S.A. Korili, A. Gil, Heterogeneous Fenton- and photo-Fenton-like catalytic degradation of emerging pollutants using Fe2O3/TiO2/pillared clays synthesized from aluminum industrial wastes, J. Water Process Eng. 52 (2023), https://doi.org/10.1016/j.jwpe.2023.103494.

[57] S. Puri, A. Verma, Color removal from secondary treated pulp & paper industry effluent using waste driven Fe–TiO2 composite, Chemosphere 303 (2022) 135143, https://doi.org/10.1016/j.chemosphere.2022.135143.

[58] V. Moradi, F. Ahmed, M.B.G. Jun, A. Blackburn, R.A. Herring, Acid-treated Fe-doped TiO2 as a high performance photocatalyst used for degradation of phenol under visible light irradiation, J. Environ. Sci. (China). 83 (2019) 183–194, https://doi.org/10.1016/j.jes.2019.04.002.

[59] H. Moradi, A. Eshaghi, S.R. Hosseini, K. Ghani, Fabrication of Fe-doped TiO2 nanoparticles and investigation of photocatalytic decolorization of reactive red 198 under visible light irradiation, Ultrason. Sonochem. 32 (2016) 314–319, https://doi.org/10.1016/j.ultsonch.2016.03.025.

[60] H. Nishikiori, S. Matsunaga, N. Furuichi, H. Takayama, K. Morita, K. Teshima, H. Yamashita, Influence of allophane distribution on photocatalytic activity of allophane–titania composite films, Appl. Clay Sci. 146 (2017) 43–49, https://doi.org/10.1016/j.clay.2017.05.026.

[61] H. Nishikiori, N. Kanada, R.A. Setiawan, K. Morita, K. Teshima, T. Fujii, Photoelectrochemical properties of dye-dispersing allophane-titania composite electrodes, Appl. Clay Sci. 107 (2015) 138–144, https://doi.org/10.1016/j.clay.2015.01.015.

[62] X. Li, K. Peng, H. Chen, Z. Wang, TiO2 nanoparticles assembled on kaolinites with different morphologies for efficient photocatalytic performance, Sci. Rep. 8 (2018) 1–11, https://doi.org/10.1038/s41598-018-29563-8.

[63] A. Magdziarz, J.C. Colmenares, O. Chernyayeva, D. Lisovytskiy, J. Grzonka, K. Kurzydłowski, K. Freindl, J. Korecki, Insight into the synthesis procedure of Fe3 +/TiO2-based photocatalyst applied in the selective photo-oxidation of benzyl alcohol under sun-imitating lamp, Ultrason. Sonochem. 38 (2017) 189–196, https://doi.org/10.1016/j.ultsonch.2017.03.012.

[64] H. Khan, I.K. Swati, Fe3+-doped anatase TiO2 with d-d transition, oxygen vacancies and Ti3+ centers: synthesis, characterization, UV-vis photocatalytic and mechanistic studies, Ind. Eng. Chem. Res. 55 (2016) 6619–6633, https://doi.org/10.1021/acs.iecr.6b01104.

[65] C. Adán, A. Bahamonde, I. Oller, S. Malato, A. Martínez-Arias, Influence of iron leaching and oxidizing agent employed on solar photodegradation of phenol over nanostructured iron-doped titania catalysts, Appl. Catal. B Environ. 144 (2014) 269–276, https://doi.org/10.1016/j.apcatb.2013.07.027.

[66] Y. Wang, J. Wang, Z. Ding, W. Wang, J. Song, P. Li, J. Liang, Q. Fan, Light promotes the immobilization of U(VI) by ferrihydrite, Molecules 27 (2022) 1–11, https://doi.org/10.3390/molecules27061859.

[67] G. Shukla, S. Angappane, Highly transparent , superhydrophilic and high-temperature stable anatase phase TiO 2, Mater. Chem. Phys. 301 (2023) 127589, https://doi.org/10.1016/j.matchemphys.2023.127589.

[68] B. Wu, W.A. Arnold, L. Ma, Photolysis of atrazine: role of triplet dissolved organic matter and limitations of sensitizers and quenchers, Water Res. 190 (2021), https://doi.org/10.1016/j.watres.2020.116659.

[69] J.A. Khan, X. He, N.S. Shah, H.M. Khan, E. Hapeshi, D. Fatta-Kassinos, D.D. Dionysiou, Kinetic and mechanism investigation on the photochemical degradation of atrazine with activated H2O2, S2O82- and HSO5-, Chem. Eng. J. 252 (2014) 393–403, https://doi.org/10.1016/j.cej.2014.04.104.

[70] Y. Li, J. Sun, S.P. Sun, Comparison of metoprolol degradation by FeIII-NTA modified Fenton-like reaction in the absence and presence of manganese: efficiency and intermediates, Chem. Eng. J. 313 (2017) 769–776, https://doi.org/10.1016/j.cej.2016.12.098.

[71] S. Talwar, A.K. Verma, V.K. Sangal, Synergistic degradation employing photocatalysis and photo-Fenton process of real industrial pharmaceutical effluent utilizing the Iron-Titanium dioxide composite, Process Saf. Environ. Prot. 146 (2021) 564–576, https://doi.org/10.1016/j.psep.2020.11.029.

[72] N. Yang, Y. Liu, J. Zhu, Z. Wang, J. Li, Study on the efficacy and mechanism of Fe-TiO2 visible heterogeneous Fenton catalytic degradation of atrazine, Chemosphere 252 (2020), https://doi.org/10.1016/j.chemosphere.2020.126333.

[73] G. Liao, C. Li, S.-Y. Liu, B. Fang, H. Yang, Emerging frontiers of Z-scheme photocatalytic systems, Trends Chem 4 (2022) 111–127, https://doi.org/10.1016/J.TRECHM.2021.11.005.

[74] D. Spasiano, R. Marotta, S. Malato, P. Fernandez-Ibañez, I. Di Somma, Solar photocatalysis: materials, reactors, some commercial, and pre-industrialized applications. A comprehensive approach, Appl. Catal. B Environ. 170–171 (2015) 90–123, https://doi.org/10.1016/j.apcatb.2014.12.050.

[75] G.A. Ortega-Moreno, S.C. Ayala-Durán, B.P. Barbero, G.E. Narda, M.C. Bernini, R.F. Pupo Nogueira, Photo-Fenton degradation of sulfamethoxazole using MIL-53(Fe) under UVA LED irradiation and natural sunlight, J. Environ. Chem. Eng. 10 (2022), https://doi.org/10.1016/j.jece.2022.107678.

[76] L.C. Mahlalela, C. Casado, J. Marugán, S. Septien, T. Ndlovu, L.N. Dlamini, Photocatalytic degradation of atrazine in aqueous solution using hyperbranched polyethyleneimine templated morphologies of BiVO4fused with Bi2O3, J. Environ. Chem. Eng. 8 (2020) 104215, https://doi.org/10.1016/j.jece.2020.104215.

[77] L.C. Mahlalela, C. Casado, J. Marugán, S. Septien, T. Ndlovu, L.N. Dlamini, Coupling biological and photocatalytic treatment of atrazine and tebuthiuron in aqueous solution, J. Water Process Eng. 40 (2021), https://doi.org/10.1016/j.jwpe.2021.101918.

[78] S. Parra, S.E. Stanca, I. Guasaquillo, K. Ravindranathan Thampi, Photocatalytic degradation of atrazine using suspended and supported TiO2, Appl. Catal. B Environ. 51 (2004) 107–116, https://doi.org/10.1016/j.apcatb.2004.01.021.

[79] I. Khan, K. Saeed, N. Ali, I. Khan, B. Zhang, M. Sadiq, Heterogeneous photodegradation of industrial dyes: an insight to different mechanisms and rate affecting parameters, J. Environ. Chem. Eng. 8 (2020), https://doi.org/10.1016/j.jece.2020.104364.

[80] M. Tariq, J. Khan, Inquest of efficient photo-assist advanced oxidation processes (AOPs) for removal of azo dye (acid yellow 17) in aqueous medium: a comprehensive study on oxidative decomposition of AY 17, SN Appl. Sci. 2 (2020), https://doi.org/10.1007/s42452-020-03701-2.

[81] K. Chunli, P. Fei, G. Jing, G. Ping, X. Honghai, Degradation of acetic acid by UV/H2O2 reaction, 3rd Int. Conf. Bioinforma. Biomed. Eng. ICBBE (2009) 3–6, https://doi.org/10.1109/ICBBE.2009.5162575 (2009.

[82] A. Verma, A.P. Toor, P. Bansal, V. Sangal, A. Sobti, TiO2-Assisted Photocatalytic Degradation of Herbicide 4-Chlorophenoxyacetic Acid: Slurry and Fixed-Bed Approach, Springer Singapore, 2019, https://doi.org/10.1007/978-981-13-6717-5_14.